JCI insight

# Altered X-chromosome inactivation in T cells may promote sex-biased autoimmune diseases

Camille M. Syrett, … , Michael Atchison, Montserrat C. Anguera

*JCI Insight.* 2019;4(7):e126751. https://doi.org/10.1172/jci.insight.126751.

**Research Article** **Cell biology**

Systemic lupus erythematosus (SLE) is an autoimmune disorder that predominantly affects women and is driven by autoreactive T cell–mediated inflammation. It is known that individuals with multiple X-chromosomes are at increased risk for developing SLE; however, the mechanisms underlying this genetic basis are unclear. Here, we use single cell imaging to determine the epigenetic features of the inactive X (Xi) in developing thymocytes, mature T cell subsets, and T cells from SLE patients and mice. We show that Xist RNA and heterochromatin modifications transiently reappear at the Xi and are missing in mature single positive T cells. Activation of mature T cells restores Xist RNA and heterochromatin marks simultaneously back to the Xi. Notably, X-chromosome inactivation (XCI) maintenance is altered in T cells of SLE patients and late-stage–disease NZB/W F1 female mice, and we show that X-linked genes are abnormally upregulated in SLE patient T cells. SLE T cells also have altered expression of XIST RNA interactome genes, accounting for perturbations of Xi epigenetic features. Thus, abnormal XCI maintenance is a feature of SLE disease, and we propose that Xist RNA localization at the Xi could be an important factor for maintaining dosage compensation of X-linked genes in T cells.



JCI insight

RESEARCH ARTICLE

# Altered X-chromosome inactivation in T cells may promote sex-biased autoimmune diseases

**Camille M. Syrett,[1] Bam Paneru,[1] Donavon Sandoval-Heglund,[1] Jianle Wang,[1] Sarmistha Banerjee,[1] Vishal Sindhava,[1] Edward M. Behrens,[2] Michael Atchison,[1] and Montserrat C. Anguera[1]**

[1]Department of Biomedical Sciences, School of Veterinary Medicine, University of Pennsylvania, Philadelphia, Pennsylvania, USA. [2]Division of Rheumatology, Children's Hospital of Philadelphia (CHOP), Philadelphia Pennsylvania, USA.

**Systemic lupus erythematosus (SLE) is an autoimmune disorder that predominantly affects women and is driven by autoreactive T cell–mediated inflammation. It is known that individuals with multiple X-chromosomes are at increased risk for developing SLE; however, the mechanisms underlying this genetic basis are unclear. Here, we use single cell imaging to determine the epigenetic features of the inactive X (Xi) in developing thymocytes, mature T cell subsets, and T cells from SLE patients and mice. We show that Xist RNA and heterochromatin modifications transiently reappear at the Xi and are missing in mature single positive T cells. Activation of mature T cells restores Xist RNA and heterochromatin marks simultaneously back to the Xi. Notably, X-chromosome inactivation (XCI) maintenance is altered in T cells of SLE patients and late-stage–disease NZB/W F1 female mice, and we show that X-linked genes are abnormally upregulated in SLE patient T cells. SLE T cells also have altered expression of XIST RNA interactome genes, accounting for perturbations of Xi epigenetic features. Thus, abnormal XCI maintenance is a feature of SLE disease, and we propose that Xist RNA localization at the Xi could be an important factor for maintaining dosage compensation of X-linked genes in T cells.**

## Introduction

About 80% of autoimmune disorders exhibit a female bias (1), including systemic lupus erythematosus (SLE), where 85% of patients are women. Additional copies of an X-chromosome (XX, XXY, XXX) are associated with increased risk for SLE and Sjögren's syndrome (2), and Turner syndrome patients (XO) have reduced risk for SLE (3). The X-chromosome is important for normal immune pathways and in the development of autoimmunity (4), as it is enriched for immunity-related genes (5) — including *TLR7* and *CD40LG*, which are frequently overexpressed in female lymphocytes from autoimmune patients (6–9). Increased dosage of *Tlr7*, arising from translocations or transgenes, is associated with lupus-like phenotypes in mice (10–12). However, the importance of mechanisms underlying X-chromosome dosage for SLE disease development or disease severity have yet to be elucidated.

Females use X-chromosome inactivation (XCI) for dosage compensation of X-linked genes between the sexes, where either the paternal or maternal X is randomly chosen for silencing in each cell. XCI is initiated during early female mammalian embryonic development (13), by allele-specific upregulation of the long noncoding RNA Xist from the future inactive X (Xi) (14–16). Xist RNA functions in *cis* to recruit chromatin complexes that deposit heterochromatic modifications such as H3K27me3 and H2a-ubiquitin across the X, resulting in transcriptional silencing (17–19). During XCI maintenance, these epigenetic modifications are enriched on the Xi and maintain transcriptional silencing of the Xi throughout the cell cycle and after cell division, to ensure dosage compensation of X-linked genes. In differentiating embryonic stem cells, *Xist* is continuously expressed from the Xi throughout the cell cycle, and Xist RNA remains tethered to the Xi of its origin throughout mitosis (20).

The majority of somatic cells maintain XCI with continuous expression of *Xist* from the Xi, and enrichment of Xist RNA transcripts and heterochromatin marks on the Xi are cytologically visible. Surprisingly, we have shown that mature naive T and B cells from female mice and humans lack these

**Conflict of interest:** The authors have declared that no conflict of interest exists.



**Submitted**: December 11, 2018
**Accepted:** February 14, 2019
**Published:** April 4, 2019.

**Reference information:** *JCI Insight.* 2019;4(7):e126751. https://doi.org/10.1172/jci.insight.126751.

epigenetic modifications on the Xi, but that Xist RNA and H3K27me3 simultaneously return to the Xi following in vitro activation (21, 22). We also found that Xist RNA first disappears from the Xi at the pro–B cell stage of B cell development in BM and that heterochromatin marks are progressively lost from the Xi during B cell differentiation (23). Here, we characterized the Xist RNA and H3K27me3 enrichment on the Xi during T cell development in the thymus, and we examined the epigenetic features of the Xi in specific $CD4^+$ T cell subsets, using in vitro and in vivo activation approaches. Remarkably, Xist RNA localization to the Xi is perturbed in T cells from a classic female-biased mouse model of SLE and female SLE patients. Gene expression profiling of SLE patient T cells revealed abundant transcriptional upregulation from the X-chromosome and aberrant expression of XIST RNA binding proteins. Together, these data reveal that the T cell lineage maintains XCI dynamically and that perturbations in Xist RNA localization affect X-linked gene expression during autoimmunity.

## Results

*Xist RNA and H3K27me3 are gradually lost from the Xi during T cell differentiation in the thymus*. Xist RNA and the heterochromatin modification H3K27me3 are enriched on the Xi in hematopoietic stem cells (HSCs) and common lymphoid progenitors (CLPs); however, these marks are missing in peripheral T cells (21, 23). To determine the developmental stage at which these modifications are lost from the Xi, we isolated thymocytes of female mice using FACS. Sorted cells were immediately fixed and used for Xist RNA fluorescence in situ hybridization (FISH) with labeled short oligo probes. We previously classified the Xist RNA localization patterns of lymphocytes into 4 groups: Type I cells have robust Xist RNA localized on the Xi; Type II cells have diffuse Xist RNA signals within a nuclear territory encompassing the X-chromosome; Type III cells have Xist RNA pinpoints across the nucleus; and Type IV cells lack Xist RNA signals (Supplemental Figure 1; supplemental material available online with this article; https://doi.org/10.1172/jci.insight.126751DS1) (21, 23). We found that double negative 1 (DN1) thymocytes ($CD4^-$, $CD8^-$, $CD25^-$, $CD44^+$) bore a mixture of Type III and Type IV Xist RNA localization patterns (Figure 1, A–C), remarkably different from BM-derived HSCs and CLPs, which are 80% Type I and -II (23). Curiously, Type I and -II Xist RNA patterns were abundant in DN2 ($CD4^-$, $CD8^-$, $CD44^+$, $CD25^+$) and DN3 thymocytes ($CD4^-$, $CD8^-$, $CD44^-$, $CD25^+$), while Type III Xist RNA patterns predominated in DN4 thymocytes ($CD4^-$, $CD8^-$, $CD44^-$, $CD25^-$), and a mixture of Type III and -IV appeared in double positive (DP) thymocytes (Figure 1C).

Next, we examined whether changes with Xist RNA localization at the Xi correlated with the disappearance of heterochromatin marks at the Xi in developing thymocytes. We performed sequential Xist RNA FISH and immunofluorescence (IF) for the heterochromatin mark H3K27me3 in DN1–4 populations and DP thymocytes. DN1 cells mostly lacked H3K27me3 foci, and we detected a focus in about 5%–8% of cells (Figure 1, D and E), consistent with reduced Xist RNA localization at the Xi. DN2 and DN3 thymocytes exhibited the strongest colocalization of H3K27me3 and Xist RNA (30%–55%), while the more mature DN4 cell population only exhibited 10% colocalization and DP cells lacked both marks (Figure 1, D and E, and Supplemental Figure 2). We next examined Xist RNA and H3K27me3 localization patterns for mature thymic single positive $CD4^+$ and $CD8^+$ thymocytes. $CD4^+$ and $CD8^+$ T cells were predominantly Type III/IV (Figure 1, F and G), similar to resting splenic T cells (21), yet $CD8^+$ T cells had more Xist RNA signals (15%–18% Type I and -II) (Figure 1, F and G). Using sequential Xist RNA FISH and IF, we observed similar low levels of Xist RNA and H3K27me3 colocalization in mature thymocytes (10%), and the majority of cells (70%) lacked both of these modifications on the Xi (Figure 1G). In sum, the Xi undergoes dynamic epigenetic changes during thymocyte development, and localization of Xist RNA correlates with H3K27me3 enrichment at the Xi.

*Xist RNA and H3K27me3 are localized concurrently at the Xi during in vitro activation of mature T cells*. Naive B cells lack Xist RNA localization on the Xi, and Xist RNA transcripts return to the Xi in 2 phases within the first 24 hours after in vitro stimulation (23). Here, we determined the kinetics for Xist RNA localization during mature splenic T cell activation using CD3/CD28. We used negative selection to isolate bulk $CD3^+$ T ($CD4^+$, $CD8^+$) cells from spleens of female mice. Cells were activated in culture with CD3/CD28 and collected cells every 24 hours for 4 days. We found that resting naive bulk T cells completely lacked detectible Xist RNA signals and were predominantly Type IV (Figure 2, A and B). Type I and -II Xist RNA patterns were most prominent at days 2 and 3 after stimulation in splenic T cells (Figure 2, A and B), while by day 4, the percentages of Type I and -II patterns decreased and Type III patterns increased (Figure 2, A and B). To further refine

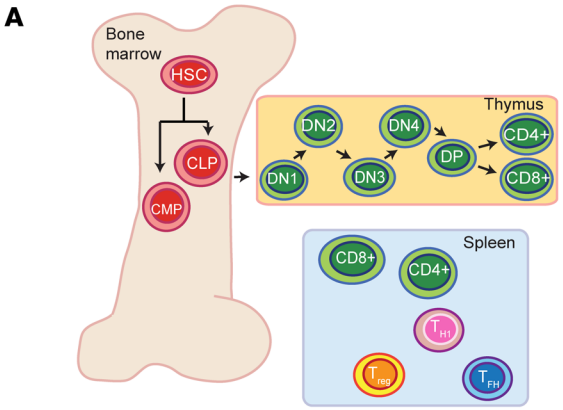
A
Bone marrow
HSC
CLP
CMP
Thymus
DN2
DN4
CD4+
DP
DN1
DN3
CD8+
Spleen
CD8+
CD4+
TH1
Treg
TFH

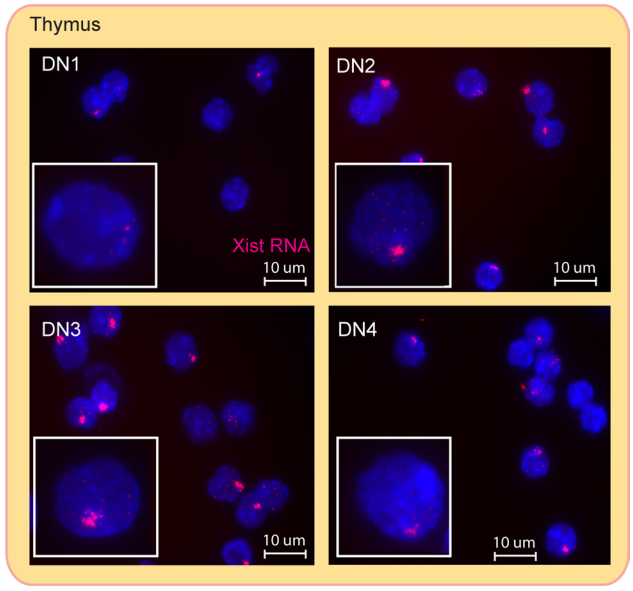
B
Thymus
DN1
Xist RNA
10 um
DN2
10 um
DN3
10 um
DN4
10 um

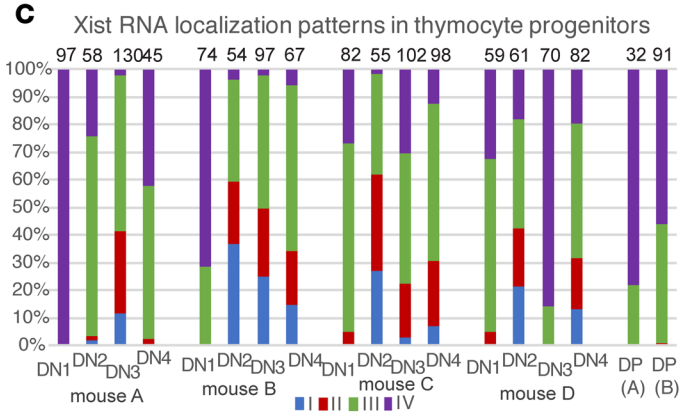
C
Xist RNA localization patterns in thymocyte progenitors
97 58 13045
74 54 97 67
82 55 102 98
59 61 70 82
32 91
100%
90%
80%
70%
60%
50%
40%
30%
20%
10%
0%
DN1 DN2 DN3 DN4
mouse A
DN1 DN2 DN3 DN4
mouse B
DN1 DN2 DN3 DN4
mouse C
DN1 DN2 DN3 DN4
mouse D
DP (A)
DP (B)
I II III IV

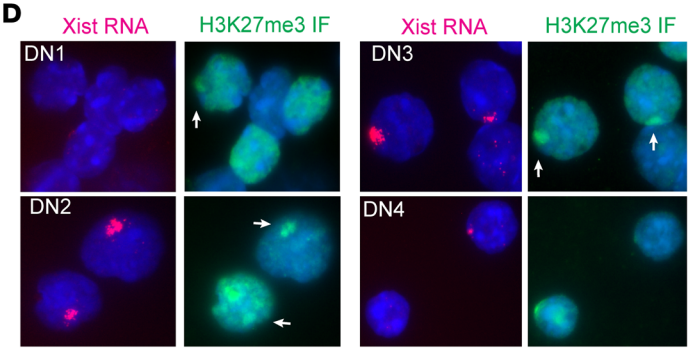
D
Xist RNA
H3K27me3 IF
Xist RNA
H3K27me3 IF
DN1
DN3
DN2
DN4

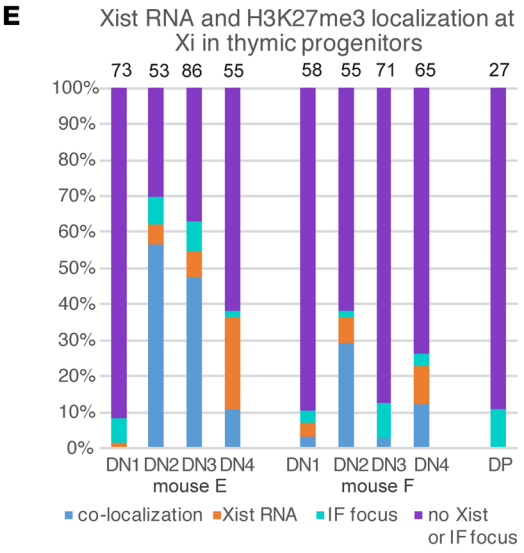
E
Xist RNA and H3K27me3 localization at Xi in thymic progenitors
73 53 86 55
58 55 71 65
27
100%
90%
80%
70%
60%
50%
40%
30%
20%
10%
0%
DN1 DN2 DN3 DN4
mouse E
DN1 DN2 DN3 DN4
mouse F
DP
co-localization
Xist RNA
IF focus
no Xist or IF focus

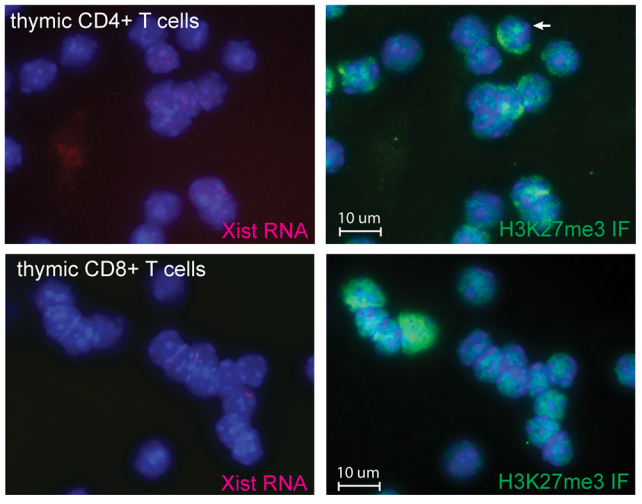
F
thymic CD4+ T cells
Xist RNA
10 um
H3K27me3 IF
thymic CD8+ T cells
Xist RNA
10 um
H3K27me3 IF

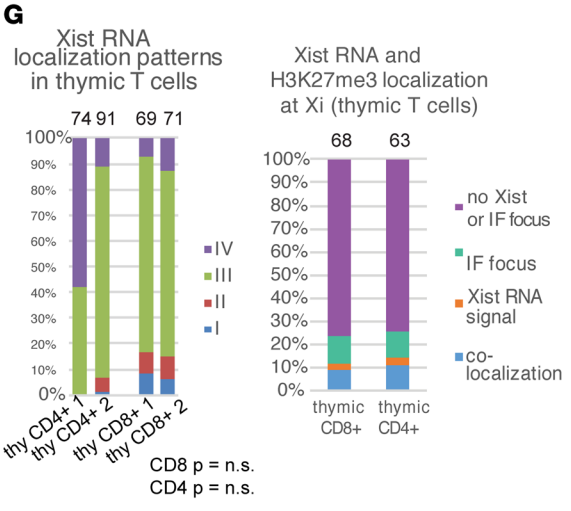
G
Xist RNA localization patterns in thymic T cells
74 91
69 71
100%
90%
80%
70%
60%
50%
40%
30%
20%
10%
0%
IV
III
II
I
thy CD4+ 1
thy CD4+ 2
thy CD8+ 1
thy CD8+ 2
CD8 p = n.s.
CD4 p = n.s.
Xist RNA and H3K27me3 localization at Xi (thymic T cells)
68
63
thymic CD8+
thymic CD4+
no Xist or IF focus
IF focus
Xist RNA signal
co-localization

**Figure 1. Xist RNA and heterochromatin marks disappear from the Xi during T cell development.** (**A**) Schematic of thymocyte differentiation in BM and thymus, as well as mature T cell subsets in the spleen. (**B**) Representative Xist RNA FISH images of nuclei from each thymocyte subset. (**C**) Quantification of Xist RNA localization patterns from each stage of thymocyte development. Results from 4 different female mice (mice A–D) are shown. Numbers above each column indicate number of nuclei counted. Statistical significance for each type of Xist RNA localization pattern across DN1-DP was determined using 1-way ANOVA; there was no statistically significant difference across all groups. (**D**) Sequential Xist RNA FISH and IF for H3K27me3 for DN1–4 (DP thymocytes shown in Supplemental Figure 2). White arrows denote H3K27me3 foci. (**E**) Quantification of colocalization patterns for Xist RNA and H3K27me3 at the Xi. Colocalization of Xist RNA and H3K27me3 focus (blue bars), Xist RNA signals alone (orange), nuclei without either signals (purple), or H3K27me3 focus (green). Numbers above each column indicate number of nuclei counted. Results from 2 different mice (mice E and F) are shown. Statistical significance for each type of Xist RNA/H3K27me3 colocalization pattern across DN1–4 was determined using 1-way ANOVA; there was no statistically significant difference across all groups. (**F**) Sequential Xist RNA FISH and H3K27me3 in mature thymic $CD4^+$ and $CD8^+$ T cells. (**G**) Quantification of Xist RNA localization patterns for thymic $CD4^+$ and $CD8^+$ T cells (left). Results from 2 different mice (labeled 1 and 2) are shown. Quantification of colocalization patterns for Xist RNA and H3K27me3 in mature thymic T cells from 1 female mouse (right). Numbers above each column indicate number of nuclei counted. Statistical significance for each type of Xist RNA localization pattern was determined using 1-way ANOVA; there was no statistically significant difference across all groups.

the timing of these events, we repeated the stimulation time course with additional collection time points between days 1–3. Xist RNA signals (Type III) first appeared at 30–36 hours after stimulation (Figure 2, C and D), which coincides with the first cell division after stimulation of mature T cells (24). We found that Type I/II patterns first appeared at 48 hours after stimulation and peaked at 72 hours (Figure 2, C and D). Thus, Xist RNA localization to the Xi during T cell stimulation occurs in 1 phase, with Xist RNA pinpoints first appearing within a small nuclear territory at 30 hours after stimulation and additional Xist RNA transcripts appearing in this region with time.

We next asked whether Xist RNA localization to the Xi during stimulation occurred simultaneously with H3K27me3 enrichment during T cell stimulation by performing sequential Xist RNA FISH and IF for H3K27me3. We quantified the number of cells with (a) an Xist RNA signal (Type I, -II, or -III), (b) with a H3K27me3 focus, (c) colocalization of both epigenetic marks, or (d) lack of both modifications. Mature splenic T cells at 0–30 hours after stimulation primarily lacked Xist RNA and H3K27me3 signals at the Xi, yet H3K27me3 foci were detectible in 3%–15% of nuclei (Figure 2, E and F). However, at 30 hours after stimulation, T cells with a detectable H3K27me3 focus also had evidence of Type II Xist RNA pinpoints (Figure 2E), suggesting that Xist RNA localization occurs concurrently with H3K27me3 enrichment at the Xi. We observed very few (3%–5%) cells with exclusive H3K27me3 foci in activated T cells (Figure 2, E and F). Colocalization of Xist RNA and H3K27me3 foci peaked at 48 hours after stimulation, at which time almost 50% of the T cells had both modifications, and remained relatively consistent through 72 hours (Figure 2, E and F). In sum, Xist RNA transcripts appear confined to the Xi nuclear territory during T cell activation, and the H3K27me3 foci accumulate together with Xist RNA at the Xi.

*$CD8^+$ and $CD4^+$ T cell subsets exhibit different kinetics for Xist RNA localization to the Xi.* Xist RNA localization at the Xi likely influences transcriptional repression, as preventing Xist RNA recruitment during B cell stimulation results in Type III Xist RNA patterns and upregulation of some X-linked genes (23). Therefore, we next asked whether distinct T cell subsets exhibited differences with Xist RNA localization patterns that could potentially influence X-linked gene transcription patterns. First, isolated $CD8^+$ T cells were stimulated in vitro using CD3/CD28, and activated cells were collected daily for 4 days. Unstimulated $CD8^+$ T cells and day 1–poststimulated T cells were predominantly Type III (Figure 3A). Robust Xist RNA Type I and -II patterns peaked at day 4 after stimulation, where approximately 50% of the T cells were Type I/II and the remaining were Type III (Figure 3A). Next, we determined Xist RNA localization patterns in in vitro–differentiated Th1 cells generated by culturing splenic $CD4^+$ T cells with CD3, CD28, IL-12, and anti–IL-4 for 3 days (25). Unlike $CD8^+$ T cells, we observed 25% Type I and 35% Type II Xist RNA localization patterns in day 1–activated $CD4^+$ Th1 cells, and this distribution stayed constant through day 3 (Figure 3B). Finally, we profiled Xist RNA localization patterns in mouse Tregs, generated either by in vitro culture (using anti-IL-4, anti–IFN-γ, and TGF-β1 for 3 days ; ref. 25) or purified from Foxp3-RFP mice, which yielded similar results. Unlike Th1 cells, we found that Type I and -II Xist RNA patterns increased at day 2 after stimulation and remained high at day 3 (Figure 3C). Thus, the kinetics and patterns of Xist RNA localization to the Xi varies between $CD8^+$ T cells and $CD4^+$ T cell subsets, and these differences suggest variation with transcriptional silencing efficiency across the Xi between cell types.

Next, we asked whether Xist RNA localization patterns in naive and activated peripherial T cells recapitulated the phenotypes of splenic cells acutely activated in vitro. We determined the Xist RNA localization patterns for sorted peripheral naive and activated $CD4^+$ and $CD8^+$ T cells. We used FACS to sort

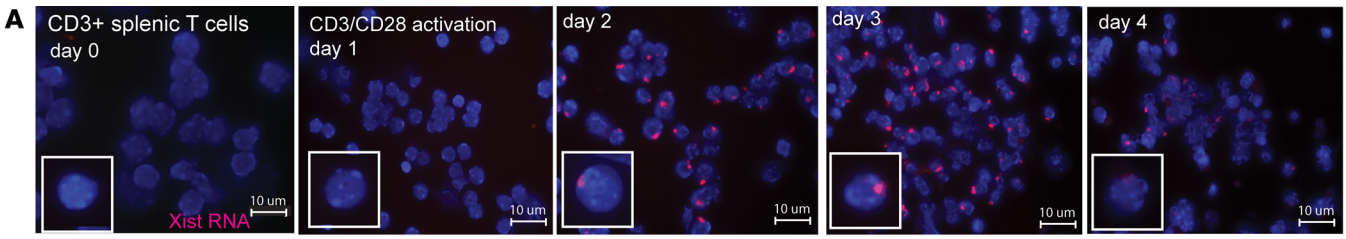
A
CD3+ splenic T cells
day 0
CD3/CD28 activation
day 1
day 2
day 3
day 4
Xist RNA
10 um

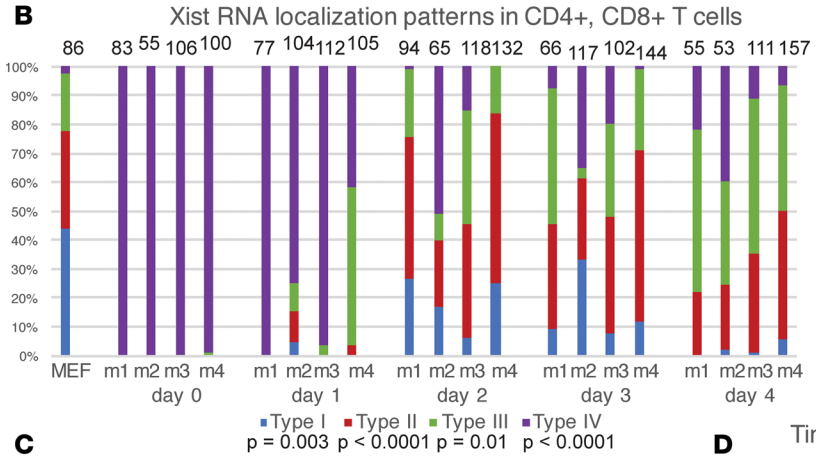
B
Xist RNA localization patterns in CD4+, CD8+ T cells
86 83 55 106 100 77 104 112 105 94 65 118 132 66 117 102 144 55 53 111 157
100%
90%
80%
70%
60%
50%
40%
30%
20%
10%
0%
MEF m1 m2 m3 m4 m1 m2 m3 m4 m1 m2 m3 m4 m1 m2 m3 m4 m1 m2 m3 m4
day 0 day 1 day 2 day 3 day 4
Type I Type II Type III Type IV
p = 0.003 p < 0.0001 p = 0.01 p < 0.0001

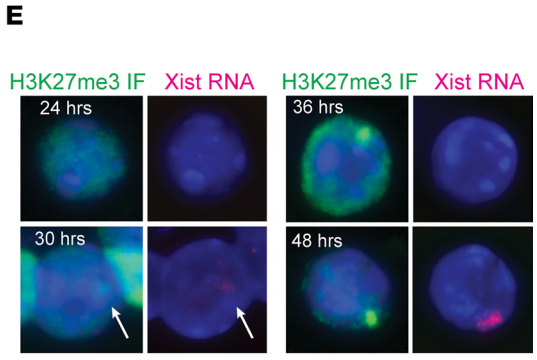
E
H3K27me3 IF Xist RNA
H3K27me3 IF Xist RNA
24 hrs
36 hrs
30 hrs
48 hrs

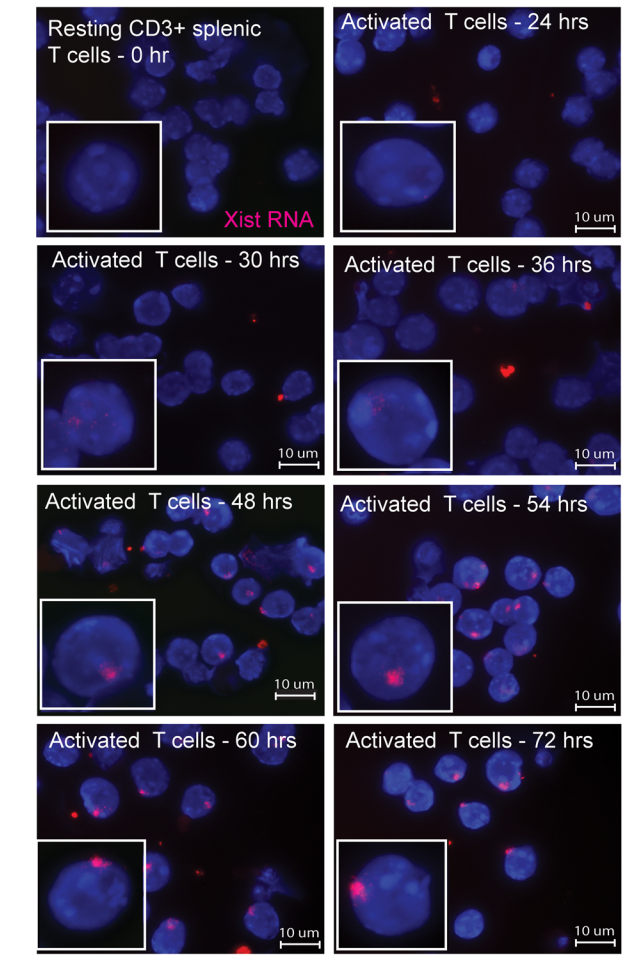
C
Resting CD3+ splenic T cells - 0 hr
Xist RNA
Activated T cells - 24 hrs
Activated T cells - 30 hrs
Activated T cells - 36 hrs
Activated T cells - 48 hrs
Activated T cells - 54 hrs
Activated T cells - 60 hrs
Activated T cells - 72 hrs
10 um

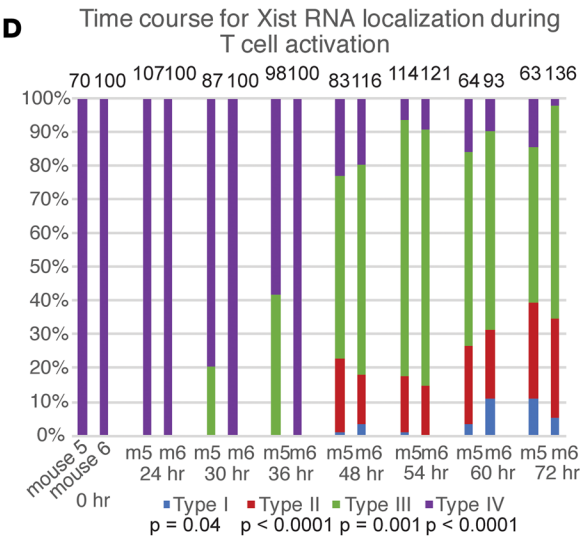
D
Time course for Xist RNA localization during T cell activation
70 100 107 100 87 100 98 100 83 116 114 121 64 93 63 136
100%
90%
80%
70%
60%
50%
40%
30%
20%
10%
0%
mouse 5 mouse 6 m5 m6 m5 m6 m5m6 m5m6 m5m6 m5m6 m5 m6
0 hr 24 hr 30 hr 36 hr 48 hr 54 hr 60 hr 72 hr
Type I Type II Type III Type IV
p = 0.04 p < 0.0001 p = 0.001 p < 0.0001

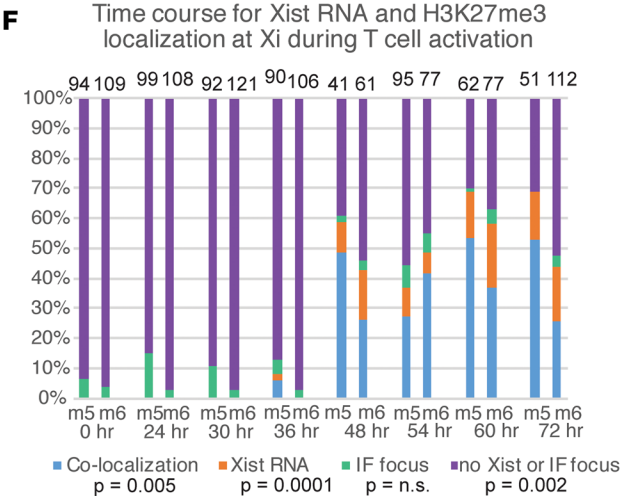
F
Time course for Xist RNA and H3K27me3 localization at Xi during T cell activation
94 109 99 108 92 121 90 106 41 61 95 77 62 77 51 112
100%
90%
80%
70%
60%
50%
40%
30%
20%
10%
0%
m5 m6 m5m6 m5m6 m5m6 m5 m6 m5m6 m5 m6 m5 m6
0 hr 24 hr 30 hr 36 hr 48 hr 54 hr 60 hr 72 hr
Co-localization Xist RNA IF focus no Xist or IF focus
p = 0.005 p = 0.0001 p = n.s. p = 0.002

**Figure 2. Timing of Xist RNA and H3K27me3 localization to the Xi during in vitro T cell stimulation.** (**A**) Time course for Xist RNA localization to the Xi for splenic CD3$^+$ T cells stimulated with CD3/CD28, determined between days 0–4. Representative results from 1 experiment are shown. (**B**) Quantification of Xist RNA localization patterns for 4 independent experiments. Statistical significance for each type of Xist RNA localization pattern across 4 different mice (labeled m1–m4) was determined using 1-way ANOVA, and *P* values for each test are shown below the graph. (**C**) Time course (24–72 hours) for Xist RNA localization at the Xi for splenic CD3$^+$ T cells stimulated with CD3/CD28. Results from 1 representative experiment are shown. (**D**) Quantification of Xist RNA localization patterns for 2 independent experiments, using 2 different mice (labeled m5 and m6). Statistical significance for each type of Xist RNA localization pattern was determined using 1-way ANOVA, and *P* values for each test are shown below the graph. (**E**) Sequential Xist RNA FISH and IF for H3K27me3 for splenic CD3$^+$ T cells at 24, 30, 36, and 48 hours after stimulation, from 1 representative experiment. Arrows indicate co-localization of Xist RNA and H3K27me3 focus. (**F**) Quantification of colocalization patterns for Xist RNA and H3K27me3 during T cell activation, using the same 2 female mice from **D**. Statistical significance for each type of Xist RNA/H3K27me3 localization pattern was determined using 1-way ANOVA, and *P* values for each test are shown below the graph.

for naive (CD62L$^{hi}$, CD44$^{lo}$) and activated (CD62$^{lo}$, CD44$^{hi}$) CD4$^+$ and CD8$^+$ T cells from preimmunized mouse spleens (Figure 4A). We found that the Type III Xist RNA pattern predominated for both naive and activated CD8$^+$ and CD4$^+$ T cells (Figure 4B). Xist RNA patterns for naive CD4$^+$ and CD8$^+$ T cells resembled resting splenic T cells (Figure 2 and Figure 3), with detectible Xist RNA signals dispersed across the nucleus (Type III) (Figure 4B). However, activated T cells from preimmunized mice had fewer Type I/II Xist RNA patterns compared with in vitro–activated T cells (Figure 4B), suggesting relaxed transcriptional silencing of the Xi. Finally, we investigated Xist RNA patterns for naive and activated CD4$^+$ T cells from mice immunized using NP-ovalbumin (NP-OVA) (Figure 4C). Surprisingly, naive and stimulated CD4$^+$ T cells after immunization had nearly identical distributions of Xist RNA localization patterns and were predominantly Type III (Figure 4D). Because we sampled 1 time point after immunization, it is possible that Type I/II Xist RNA patterns are generated in vivo but occur with different kinetics than in vitro cells. Finally, we also isolated CD4$^+$ T follicular helper cells (Tfh) from immunized mice using FACS (Figure 4C). Tfh cells exhibited predominantly Type III (90%) Xist RNA patterns, similar to CD4$^+$ T cells (Figure 4D). In sum, Xist RNA is dispersed across the nucleus in the majority of CD4$^+$ and CD8$^+$ T cells isolated from spleen, irrespective of activation status in vivo, and suggests relaxed fidelity of Xi transcriptional silencing.

*Xist RNA becomes mislocalized from the Xi during late-stage lupus disease in NZB/W F1 mice and pediatric SLE patient T cells*. NZB x NZW F1 (NZB/W F1) mice are a classic mouse model for spontaneous lupus-like disease that exhibits a strong female bias, where animals produce elevated serum anti-dsDNA and develop immune complex-mediated glomerulonephritis resulting in kidney failure and death within 6–12 months. The female bias for disease development has been partially attributed to estrogen levels because ovariectomized NZB/W F1 mice have delayed disease onset and reduced autoantibody levels (26); however, the genetic contribution from the X-chromosome has not been carefully examined. One feature of lupus disease common to both NZB/W F1 mice and human SLE patients is CD4$^+$ T cell–driven B cell hyperactivity and autoantibody production (27). Here, we asked whether perturbations with XCI maintenance are observed in female T cells from NZB/W F1 mice at 3 stages: predisease, early-stage disease, and late-stage as assessed by proteinuria levels. We isolated splenic T cells from predisease (0 or + proteinuria), early-stage–disease moderate (moderate [+/++] proteinuria), and late-stage–disease high (high [+++/++++] proteinuria) female NZB/W F1 mice, and we used age-matched WT mice (BALB/c and C57BL/6 strains) as controls. We activated cells in vitro using CD3/CD28 and collected cells for Xist RNA FISH analyses at days 0, 2, and 3 after stimulation. The Xist RNA localization patterns for NZB/W F1 naive and stimulated T cells resembled age-matched WT controls for predisease and early-stage–disease mice (Supplemental Figure 3, A and B). However, Xist RNA patterns from both naive and in vitro–activated T cells from late-stage–disease NZB/W F1 mice were significantly different from WT animals. Naive T cells from late-stage–disease NZB/W F1 female mice had detectible Xist RNA nuclear signals (40% Type III Xist RNA patterns; $P < 0.0001$), while WT animals uniformly lacked Xist RNA signals (100% Type IV) (Figure 5, A and C). For activated T cells, we observed more dispersed Xist RNA patterns in late-stage–disease NZB/W F1 T cells and fewer Type I and II patterns (Figure 5, B and C; $P = 0.02$ and $P < 0.0001$). Thus, Xist RNA becomes mislocalized from the Xi during late-stage disease for naive and activated T cells of NZB/W F1 mice, suggesting partial reactivation on this chromosome.

To determine whether Xist RNA mislocalization is a feature of human SLE, we examined XIST RNA localization patterns in peripheral and in vitro–activated T cells from pediatric SLE patients and age-matched controls. T cells were isolated from PBMCs from SLE patients in disease remission (SLE disease activity index [SLEDAI] score 0–1) recruited from CHOP, stimulated in vitro using CD3/CD28, and then

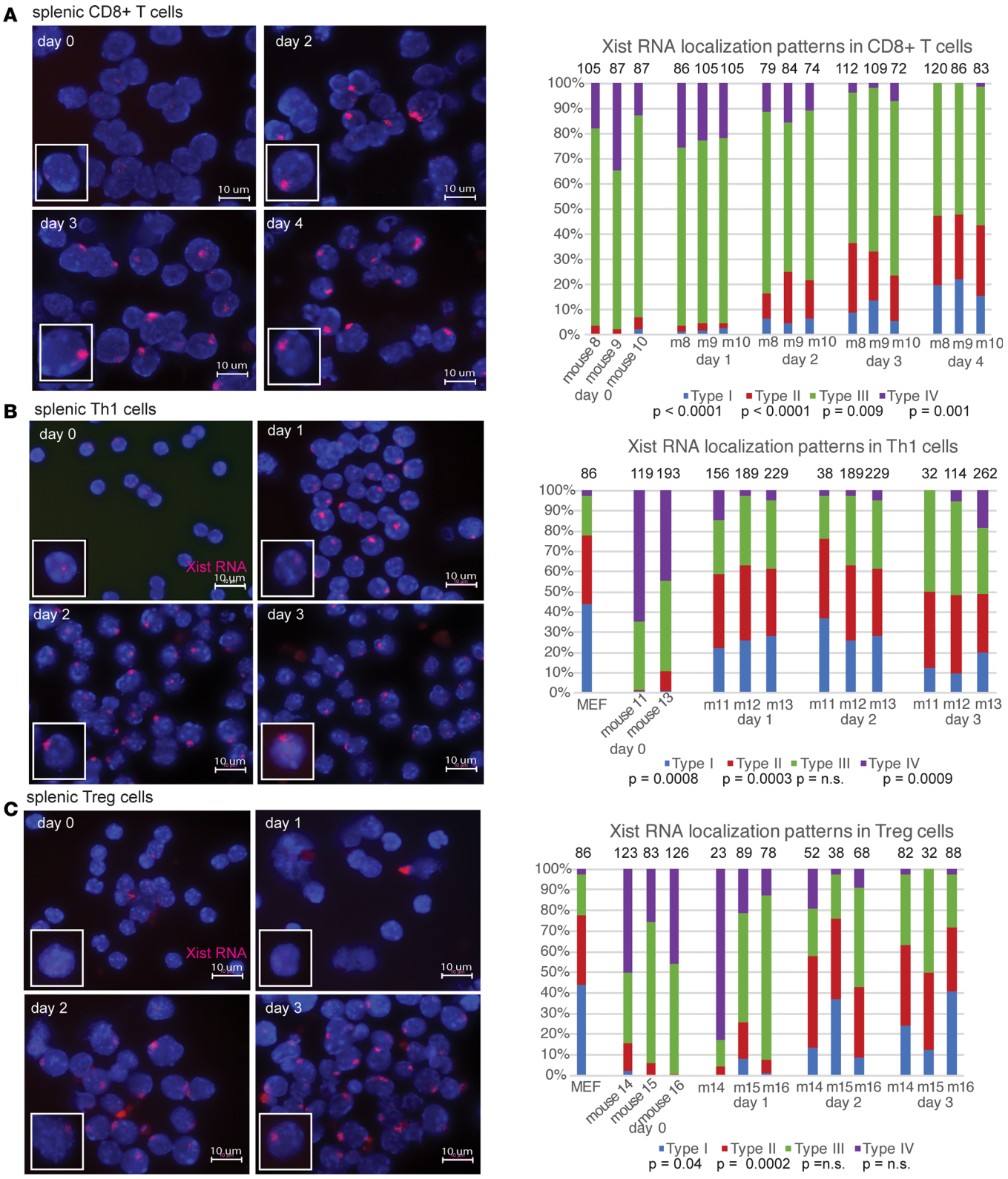


**Figure 3. Xist RNA localization patterns in CD8⁺ T cells and CD4⁺ T cell subsets.** (**A**) Xist RNA FISH for splenic CD8⁺ T cells stimulated for 4 days using CD3/CD28, from 1 representative experiment (left). Quantification of Xist RNA localization patterns from 3 different female mice, labeled mouse 8–10 (right). Statistical significance for each type of Xist RNA localization pattern was determined using 1-way ANOVA, and *P* values for each test are shown below the graph. (**B**) Xist RNA FISH and quantification of localization patterns for splenic CD4⁺ Th1 cells, using 3 different female mice (labeled mouse 11–13). Statistical significance for each type of Xist RNA localization pattern was determined using 1-way ANOVA, and *P* values for each test are shown below the graph. (**C**) Xist RNA FISH and quantification of localization patterns for splenic Tregs isolated from 3 different female mice (labeled mouse 14–16). Statistical significance for each type of Xist RNA localization pattern was determined using 1-way ANOVA, and *P* values for each test are shown below the graph.

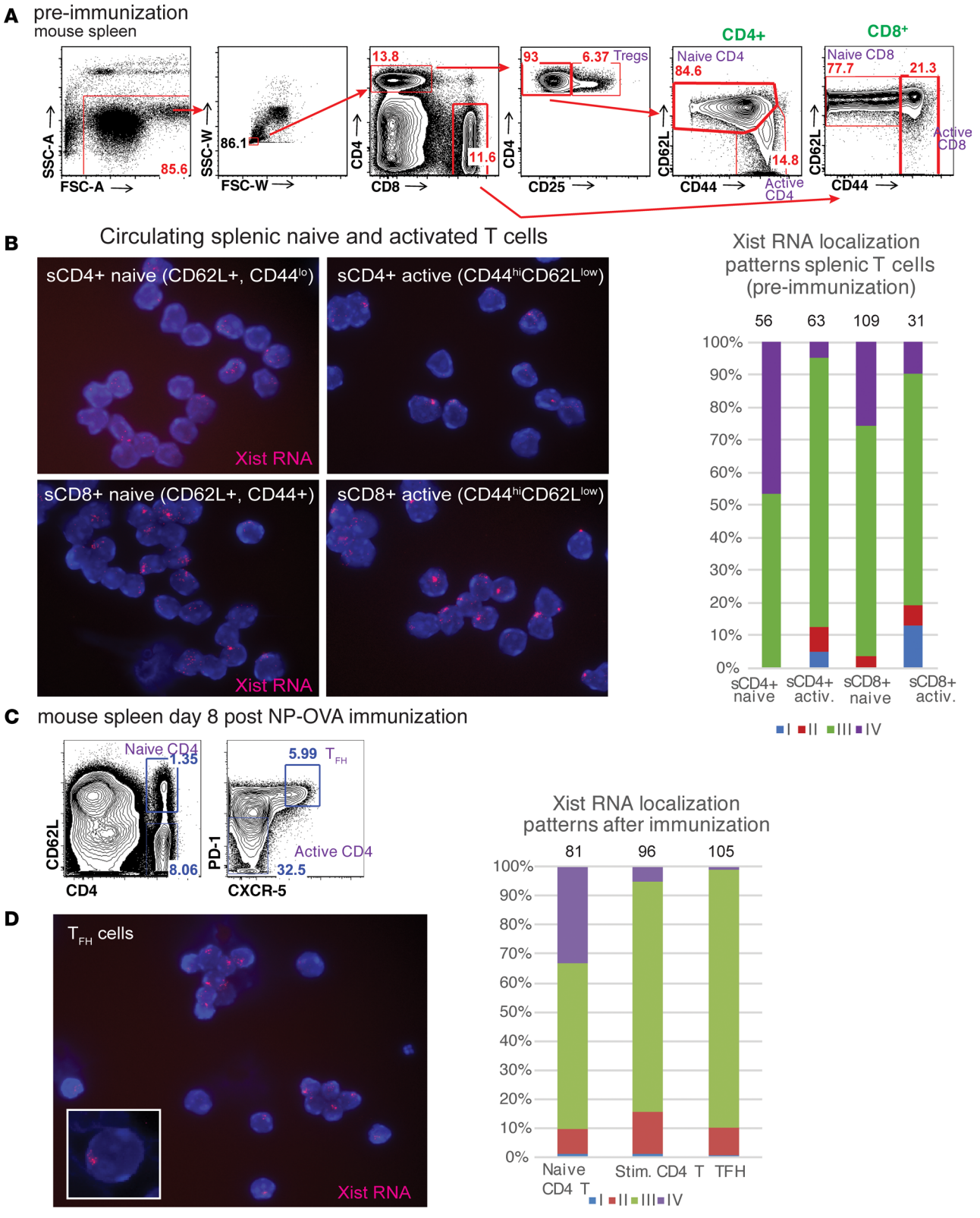


**Figure 4. Xist RNA transcripts are diffuse at the Xi for in vivo–activated T cell subsets.** (**A**) Representative FACS analysis for sorting naive and activated CD4⁺ and CD8⁺ T cells from the spleens of preimmunized mice ($n$ = 2). (**B**) Xist RNA FISH for circulating splenic (s) naive and activated CD4⁺ and CD8⁺ T cells from preimmunized mice, sorted using the gating strategy in **A** (left). Quantification of Xist RNA localization patterns for splenic CD4⁺ and CD8⁺ T cells (right). (**C**) Representative FACS analysis for sorting T follicular helper cells from mice immunized with NP-OVA. Spleens were collected at day 8 after immunization from 2 female mice. (**D**) Xist RNA FISH for T follicular helper cells (left) and quantification of Xist RNA localization patterns for CD4⁺ T cell subsets from spleens of NP-OVA–immunized mice (right).

subjected to XIST RNA FISH using human-specific fluorescently labeled oligo probes (21). We quantified the percentage of each type of XIST RNA localization pattern for both circulating and in vitro–stimulated T cells (Supplemental Figure 4). We found that peripheral T cells from SLE patients had significantly elevated levels of XIST RNA signals dispersed across the nucleus (Type III) compared with healthy controls (Figure 6, A and C; $P = 0.02$). Remarkably, in vitro–activated T cells from SLE patients in disease remission had significantly fewer Type I and -III XIST RNA patterns relative to healthy controls (Figure 6, B and C, and Supplemental Figure 4B; $P = 0.0003$ and $P = 0.02$), similar to activated T cells from disease-state NZB/W F1 mice. These results indicate that mislocalization of Xist/XIST RNA is a feature of SLE disease in mice and humans and suggest that transcriptional silencing of the Xi might be impaired.

*Female-specific overexpression profile of X-linked genes in SLE T cells and abnormal expression of XIST RNA binding proteins*. Next, we asked whether mislocalization of XIST RNA affected X-linked gene expression in SLE patient T cells. We reanalyzed RNA sequencing (RNA-seq) results from a study that collected RNA from SLE patient peripheral T cells (female and male) and healthy female controls (28), and we examined expression from the X-chromosome. Using DESeq2, we compared X-linked gene expression of 4 healthy female control samples with 10 female SLE patients, and we found that 143 X-linked transcripts were differentially expressed in SLE T cells (Supplemental Table 1). XIST expression was nearly identical between SLE and healthy control samples (Supplemental Figure 5A). Next, we compared 5 female SLE samples from patients with high SLEDAI values to healthy female samples, and we detected overexpression (at an FDR < 5%) for 79 X-linked gene transcripts (Figure 7A and Supplemental Table 2). Seventy-seven X-linked gene transcripts were downregulated, and 8 of these genes have been reported to escape XCI in various human cell types (29) (Supplemental Table 2 and Supplemental Figure 6). We repeated this comparison using 5 female SLE samples with low SLEDAI scores and female heathy controls, and we found 21 X-linked gene transcripts that were significantly upregulated and 20 downregulated transcripts (Figure 7B and Supplemental Table 3). XCI escape genes are present in both upregulated and downregulated gene transcripts (Supplemental Table 3). Comparison of the lists of transcripts uniquely upregulated in SLE patients with high SLEDAI scores (56 genes) and low SLEDAI (4 genes), revealed 16 X-linked gene transcripts that were consistently overexpressed in SLE T cells (Figure 7C and Supplemental Table 4). This list includes genes that are normally subject to XCI silencing that function in metabolism (*ARSD*, *ATP6AP1*, *G6PD*, *PDHA1*), cell cycle and proliferation (*EGFL6*, *SPIN2B*), cell division (*SEPTIN-6*), and splicing (*MBNL3*). Three of these genes escape XCI (*ARSD*, *HDHD1*, *JPX*). We also observed increased expression of the immunoregulatory gene *FOXP3*, the lineage-specific marker of Tregs that also becomes induced upon $CD4^+$ T cell activation (30) (Supplemental Table 4). Thus, the expression profile of X-chromosome becomes dynamically reorganized in SLE patient T cells, and we have identified a potentially novel gene signature for X-linked genes overexpressed in SLE patient T cells, irrespective of disease state.

To determine whether X-linked gene expression changes in SLE arise from the Xi or Active X (Xa), we compared X-linked gene expression profiles for male (XaY) and female SLE patients (XaXi) with healthy female controls. We observed that female SLE T cells overexpressed 19 X-linked transcripts compared with male SLE (Figure 7D, Supplemental Table 5, and Supplemental Table 6), including 4 immunity-related genes: *IRAK1*, *XIAP*, *TSC22D3*, and *MMP1*. Importantly, the male SLE X-linked gene expression profile for these genes resembled the female healthy controls, eliminating the possibility that overexpression is caused by disease-induced lymphocyte activation and instead arises from compromised transcriptional silencing of the Xi. Next, we determined the regions along the X-chromosome that were overexpressed in both high and low SLEDAI female SLE T cells using positional enrichment analysis. We found that the regions are distributed in both the p and q arms of the chromosome and are mostly absent from known XCI escape regions (Figure 7E). In sum, we identified a potentially novel set of T cell–specific X-linked genes overexpressed in SLE patients with varying disease severity, and we found that the majority of the overexpressed X-linked genes should be subject to XCI but may become transcribed.

We have previously reported that 2 XIST RNA interacting proteins, YY1 and hnRNP-U (SAF-A), are required for localizing Xist RNA to the Xi in activated lymphocytes (21). Thus, we asked whether the expression of known XIST RNA interacting proteins is altered in SLE patient T cells. We assembled a list of 275 Xist RNA interacting proteins taken from the literature (21, 31–34) and compared their expression with T cells from high SLEDAI SLE patients and healthy female controls. We found that 29 Xist RNA interacting protein gene transcripts were significantly upregulated in SLE samples (at FDR < 5%), and 43 genes were downregulated in SLE T cells (Figure 8 and Supplemental Table 7). The list of upregulated Xist

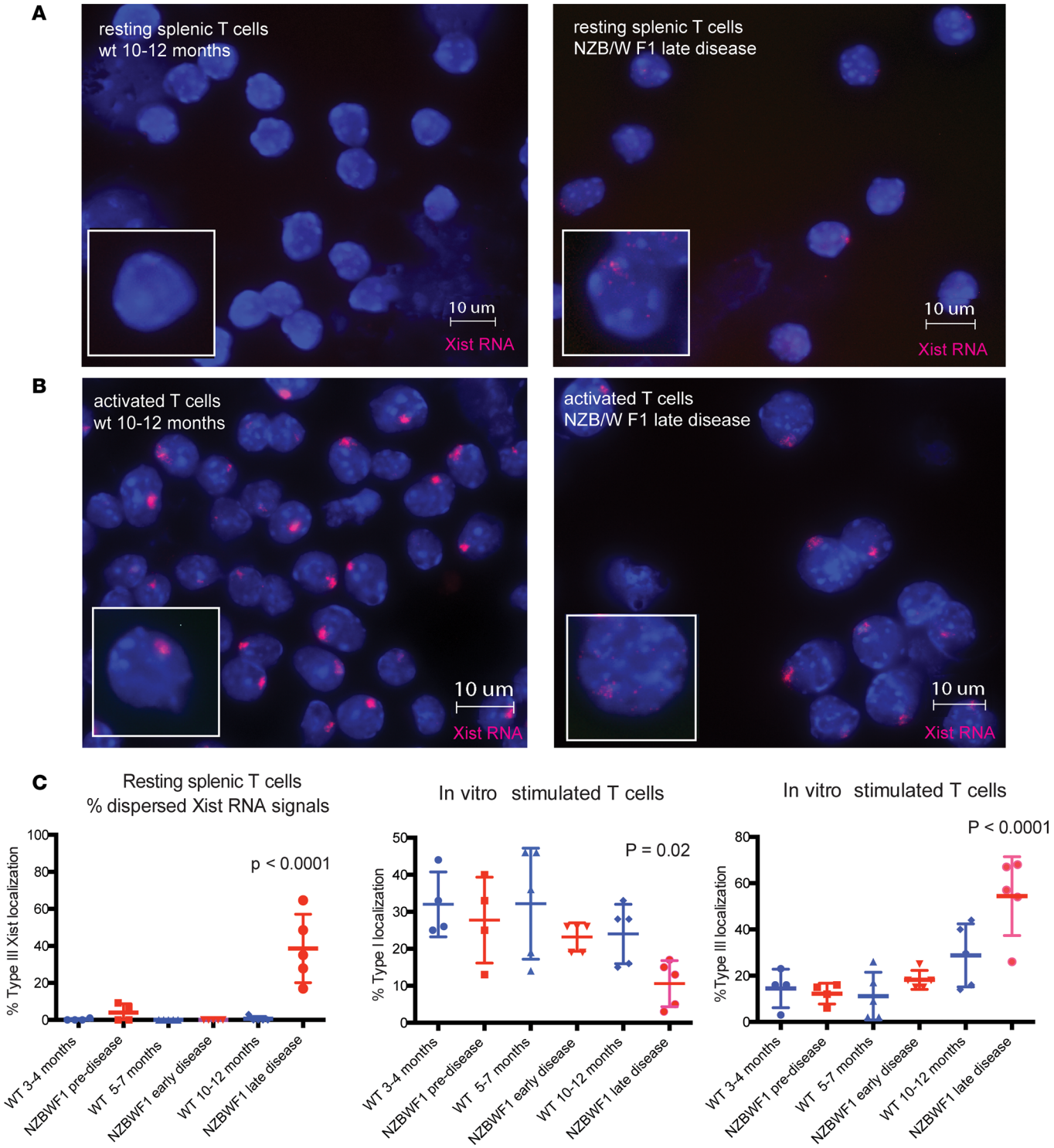


**Figure 5. Xist RNA becomes mislocalized from the Xi in T cells from diseased NZB/W F1 mice.** (**A**) Representative Xist RNA FISH images from resting splenic T cells from late-stage–disease NZB/W F1 mice (determined by proteinuria and serum dsDNA autoantibody levels) and age-matched healthy controls (C57BL/6J, BALB/c). (**B**) Representative Xist RNA FISH images from in vitro activated (CD3/CD28) splenic T cells from late-stage–disease NZB/W F1 mice and age-matched healthy controls (C57BL/6J, BALB/c). (**C**) (Left) Quantification of Type III Xist RNA localization patterns in splenic T cells from NZB/W F1 mice from 3 disease stages (predisease, early-stage disease, and late-stage disease) and age-matched controls ($n$ = 4–5 mice/group) for each disease time point. At least 23 nuclei (23–159 nuclei) were counted for each sample; total counts shown in Supplemental Figure 3. (Center and right) Quantification of Type I and Type III Xist RNA localization patterns for in vitro–activated splenic T cells. At least 50 nuclei (50–237 nuclei) were counted for each sample; total counts shown in Supplemental Figure 3. Error bars denote mean ± SD, and statistical significance was determined for each type of Xist RNA localization pattern between all groups using an ordinary 1-way ANOVA (nonparametric tests).

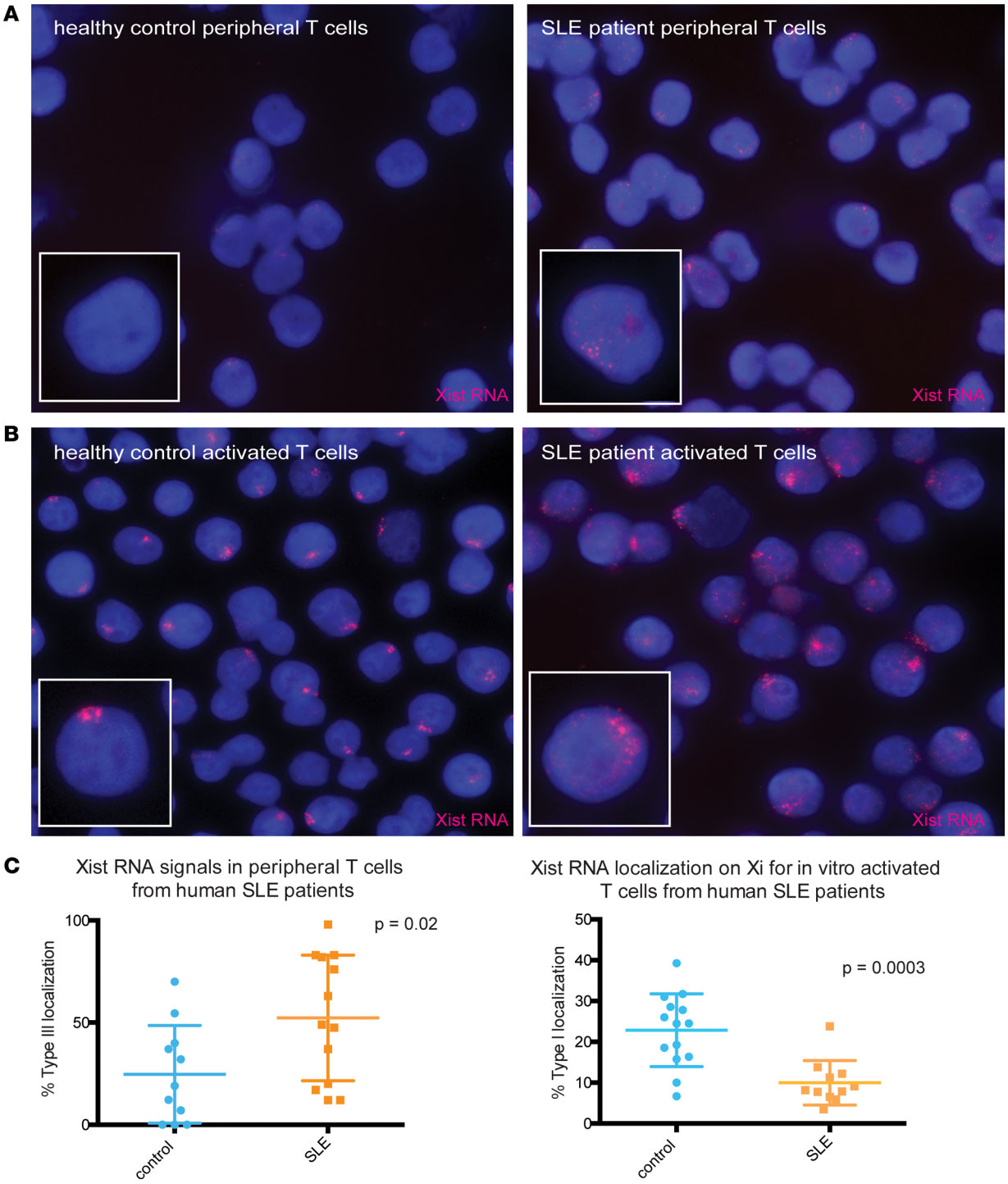


**Figure 6. Peripheral T cells from pediatric SLE patients have mislocalized XIST RNA patterns.** (**A**) Representative XIST RNA FISH images from circulating T cells from 1 SLE patient (SLEDAI 0) and age-matched control. (**B**) Representative XIST RNA FISH images for in vitro–activated T cells from 1 pediatric SLE patient and age-matched healthy control. (**C**) (Left) Quantification of Type III XIST RNA localization patterns in circulating T cells from pediatric SLE patients ($n$ = 13) and healthy age-matched controls ($n$ = 10). (Right) Quantification of Type I XIST RNA localization patterns for in vitro–activated T cells from SLE patients and healthy controls. Error bars denote mean ± SD, and statistical significance was determined using 2-tailed unpaired $t$ tests.

RNA interacting genes includes nuclear matrix proteins, splicing factors, and transcriptional regulation, as well as 1 gene (*LMNB1*) with a known role in XCI (35) (Supplemental Table 7). We found that 4 Xist RNA interacting protein genes with known roles in XCI were downregulated in SLE patient T cells: *DNMT1*, *LBR*, *SMCHD1*, and *CIZ1* (35–39). This list also included the nuclear matrix and envelope proteins, as well

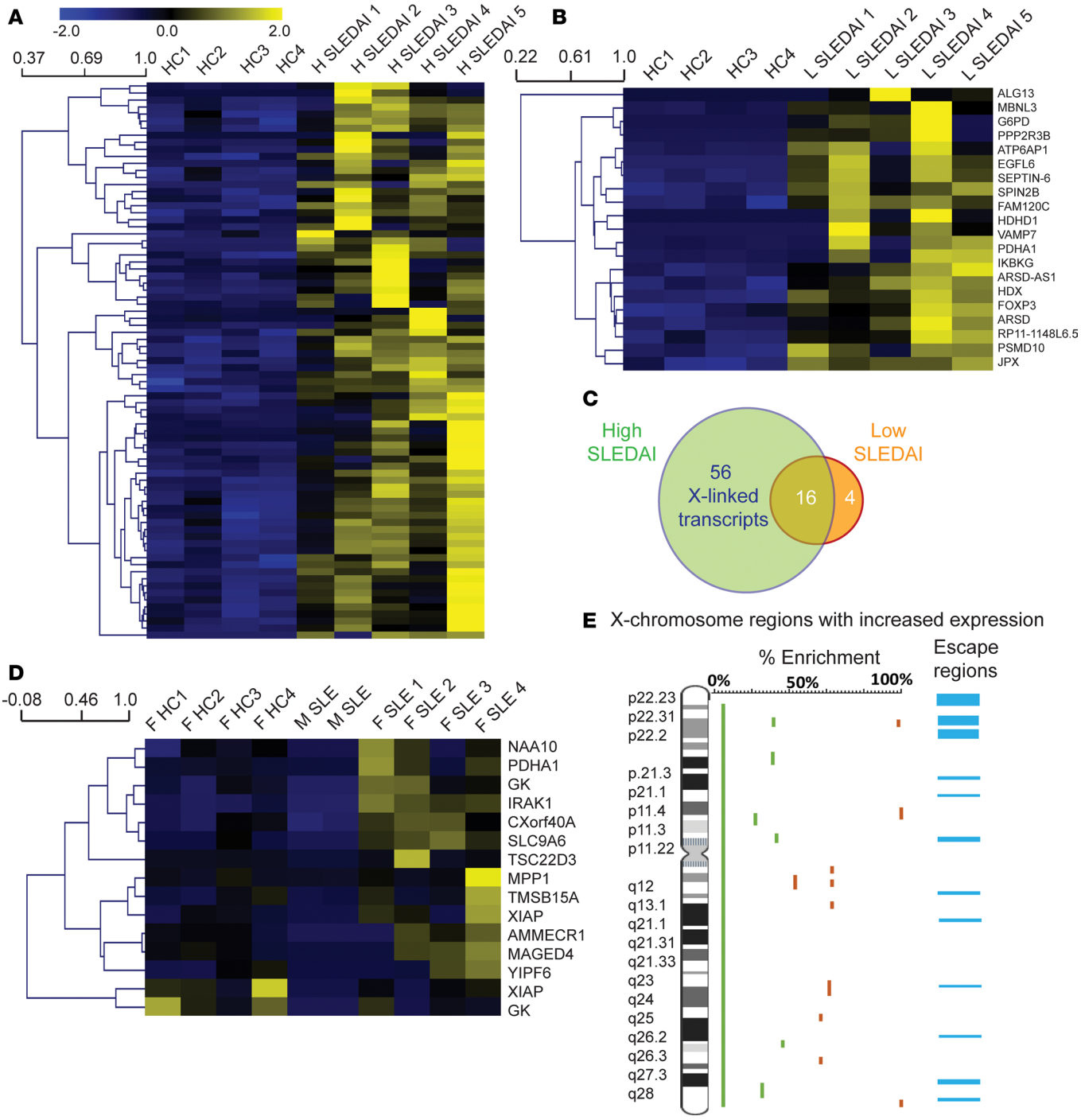


**Figure 7. Increased transcription across the X-chromosome and differential expression of XIST RNA interacting proteins in T cells from SLE patients.** (**A**) Heatmap showing X-linked gene transcripts overexpressed in T cells from 5 female SLE patients with high (H) SLEDAI scores (score 12–26) compared with 4 healthy control (HC) females. Gene transcript information is in Supplemental Table 2. (**B**) Heatmap showing X-linked gene transcripts overexpressed in 5 female SLE patients with low (L) SLEDAI scores (score 0–4) compared with HC females. Gene names for each transcript are shown; transcript IDs are listed in Supplemental Table 3. (**C**) Venn-diagram showing the number of X-linked genes overexpressed in high SLEDAI (score 12–26) and low SLEDAI (score 0–4) cases from **A** and **B**. (**D**) Heatmap of the X-linked genes overexpressed in female (F) SLE patients ($n$ = 4) compared with male (M) lupus patients ($n$ = 2) and healthy female individuals ($n$ = 4). Gene names for each transcript are shown; transcript IDs are listed in Supplemental Tables 5 and 6. (**E**) Positional gene enrichment (PGE) analysis for X-linked genes overexpressed in T cells from female SLE patients compared with female healthy controls. Regions with % enrichment > 50 are denoted in red; regions with % enrichment < 50 are shown in green. The regions along the X-chromosome containing genes that escape XCI (ref. 50) are represented in blue (right side). Statistical significance for fold changes in gene expression was determined using FDR < 0.05.

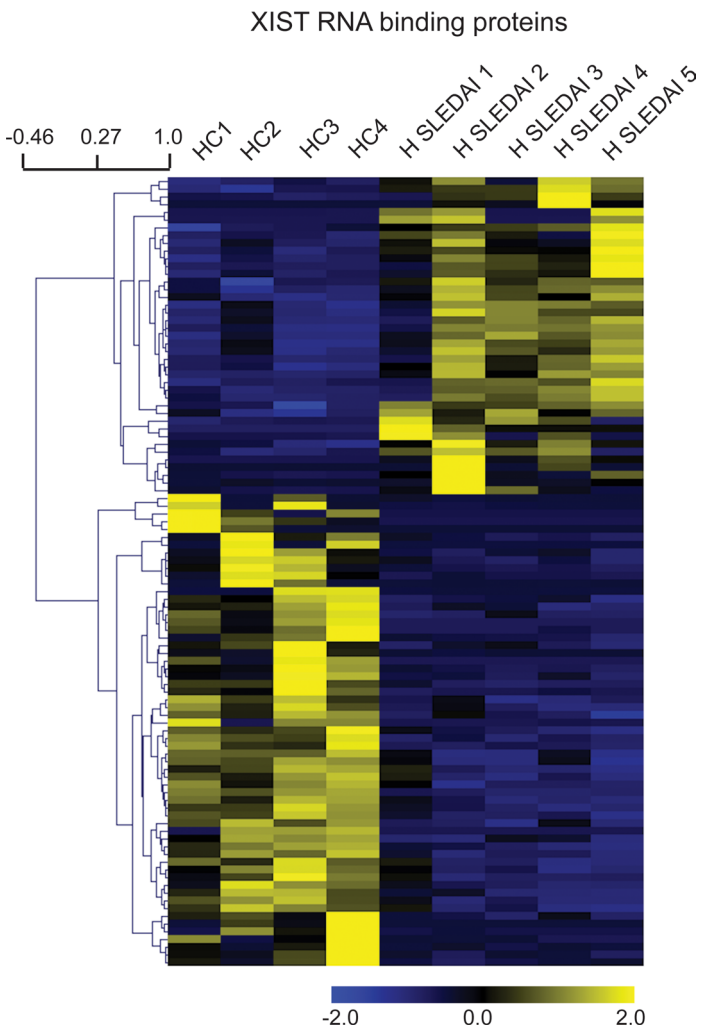


**Figure 8. Altered expression of XIST interacting proteins in SLE patient T cells.** Heatmap of differentially expressed XIST interacting protein coding genes between female SLE patients with high SLEDAI scores (score 12–26; $n$ = 5) and healthy female controls ($n$ = 4). Complete gene transcript lists of upregulated and downregulated transcripts are listed in Supplemental Table 7.

as factors involved in metabolism, cell cycle, and splicing (Supplemental Table 7). Taken together, Xist RNA interacting proteins are misregulated in SLE patient T cells, suggesting that altered transcription may contribute to the mislocalized XIST RNA patterns.

## Discussion

SLE predominantly affects females, and it is well established that (a) some X-linked genes (including *CD40LG* and *CXCR3*) are overexpressed in SLE $CD4^+$ T cells and (b) multiple X-chromosomes increases risk for this disease. Various hypotheses involving the X-chromosome have been proposed (4), including nonrandom XCI, X-chromosome loss, and X-reactivation; however, the evidence supporting these theories is lacking. In this study, we investigated the epigenetic features of the Xi during thymocyte development, in mature $CD8^+$ T cells and $CD4^+$ T cell subsets, and in SLE mouse models and patients. Our work is the first to our knowledge to demonstrate that dynamic XCI maintenance is a feature of T cell progenitors and mature T cell subsets and that XCI maintenance is disrupted in T cells from the female-biased NZB/W F1 SLE mouse model and SLE patients.

Findings presented here show that dynamic XCI maintenance of mature T cell subsets originates during thymocyte development in the thymus. Unlike HSCs and CLPs in the BM, which have abundant Xist RNA signals on the Xi (23), Xist RNA is not robustly localized on the Xi in DN1 cells, the earliest thymocyte progenitor. Curiously, Xist RNA reappears at the Xi during thymocyte development, in DN2

and DN3 thymocytes, which coincides with the rearrangement of the T cell β-chain locus and CD25 expression. Xist RNA localization diminishes at the DN4 stage, coincident with the loss of CD25 expression, and DP thymocytes predominantly lack detectable Xist RNA signal (Type IV). The significance of the correlation between Xist localization at the Xi and CD25 expression in thymocytes is unknown but is specific to T cells because transient CD25 expression at the pre–B cell stage is not associated with detectable Xist RNA signals (23). Xist RNA is transiently localized to the Xi during thymocyte maturation, but B cell progenitors lack detectable Xist RNA transcripts (23); however, the physiological significance of these differences remain unclear.

Our results suggest that the Xi becomes more euchromatic during thymocyte development, and we propose that disappearance of these epigenetic modifications from the Xi enables increased expression of some X-linked genes that may be required for T cell maturation. We observed reduced H3K27me3 enrichment on the Xi during thymocyte development, which also occurs during B cell maturation in the BM (23), suggesting that selected reactivation of X-linked genes may be important for lymphocyte development. In support, the X-linked gene *Foxp3* is transiently expressed in DN thymocytes and correlates with CD25 and CD44 expression (40). Additional experiments are necessary to determine whether expression of *Foxp3* occurs from both the Xa and Xi, and to identify the full repertoire of X-linked genes that escape XCI for T and B cell progenitors.

Our work found that the kinetics of Xist RNA localization at the Xi is different between T and B cells (23), where epigenetic modifications appear clustered at the Xi prior to the first cell division in stimulated T cells. The heterochromatic mark H3K27me3 becomes enriched at the Xi at the same time that Xist RNA signals are clustered in this nuclear area, supporting that localization of Xist RNA occurs in 1 phase. Colocalization of Xist RNA and H3K27me3 is first seen at 48 hours after stimulation, and very few nuclei lacking Xist RNA signal had an H3K27me3 focus prior to 48 hours. Our results suggest that Xist RNA may be directly recruiting PRC2 to the Xi for H3K27me3 enrichment during T cell activation, similar to models proposed for XCI initiation during mouse embryonic stem cell differentiation (19, 41). Alternatively, the Xi may contain an imprint that directs both Xist RNA and PRC2 independently to this chromosome during T cell activation. Additional experiments are necessary to determine the nature of the imprint and the mechanism for PRC2 recruitment to the Xi in mature T cells.

This study indicates that T cell subsets exhibit differences in the timing of the return of Xist RNA to the Xi. We found that resting $CD8^+$ T cells are predominantly Type III for Xist RNA localization and that Xist RNA transcripts accumulate at the Xi at days 3 and 4 after stimulation. Type I and -II Xist RNA localization patterns predominate in day 1–activated $CD4^+$ Th1 cells, and the distribution does not change over time. While Xist RNA localization at the Xi is delayed by 1 day for $CD4^+$ Tregs compared with Th1 cells, and the significance of this delay is unclear. We found that the size of the Xist RNA cloud at the Xi is smaller for in vivo–activated T cells compared with in vitro–activated cells. This size discrepancy may reflect differences with steady state levels of Xist RNA or concentrations of proteins that either localize or tether Xist RNA to the Xi. We previously reported that the nuclear matrix protein hnRNP-U and the transcription factor YY1 are required to localize XIST RNA at the Xi in activated human T cells (21). It is possible that in vivo–activated T cells have less YY1 and hnRNP-U protein compared with in vitro–activated cells, resulting in smaller Type I Xist RNA clouds, fewer Type I/II patterns, and more dispersed Type III cells. It is unclear whether fewer Xist RNA transcripts at the Xi correlates with greater gene expression from the Xi, and future experiments addressing how the density of Xist RNA transcripts across the Xi influences transcriptional repression are necessary. It is important to note that the correlation between XCI escape and Xist RNA localization patterns Type I, II, III, and IV is still unknown because activated cells contain a mixture of the 4 localization patterns. However, ex vivo deletion of YY1 in activated B cells generates a mixture of Type III and -IV cells, and we observed female-specific overexpression of 20 X-linked genes, reflecting reactivation from the Xi (23). Allele-specific transcriptional profiling of pure lymphocyte populations for each type of Xist RNA pattern are necessary to define the transcriptional consequences for each localization pattern.

Importantly, this study demonstrates that Xist RNA localization patterns are perturbed in resting and in vitro–activated T cells from female SLE patients and late-stage–disease female NZB/W F1 mice. We propose that Xist RNA mislocalization from the Xi contributes to abnormal reactivation of some, but not all, X-linked genes from the Xi. Our data demonstrate that in vitro–activated T cells from pediatric SLE patients in disease remission have dispersed XIST RNA transcripts. It is possible that abnormal XIST

RNA localization occurred as a consequence of disease progression in these patients because dispersed Xist RNA patterns were only detected in late-stage–disease NZB/W F1 T cells. Sample abundance prevented us from examining H3K27me3 or H2A-Ub enrichment on the Xi following XIST RNA FISH; therefore, it is unknown whether mislocalized XIST RNA clouds affect H3K27me3 localization. Our bioinformatic analyses of SLE patient CD4$^+$ T cell RNA-seq profiles revealed that 21 and 79 X-linked gene transcripts were upregulated in female SLE patients with low or high SLEDAI scores, respectively, supporting our hypothesis that XIST RNA mislocalization is associated with increased expression of some X-linked genes. In support, the X/autosome gene expression ratio is similar between SLE and healthy control samples (Supplemental Figure 5B), indicating that altered expression from the X is not disproportionate to the genome. Importantly, some selective X-linked gene reactivation likely occurs on the Xi because RNA-seq profiles of male SLE patient T cells resemble healthy female controls. It is possible that hormonal differences between male and female SLE patients might influence expression of some the X-linked genes that were differentially expressed in Figure 7D. The list of X-linked genes overexpressed in SLE patient T cells contain genes that are known to escape XCI (such as *KDM5C* and *JPX*) and also genes that should be transcriptionally silenced (*FOXP3* and *IL2RG*). Indeed, the X-linked genes overexpressed in SLE are found distributed across the X-chromosome and do not cluster exclusively in XCI escape regions. It is intriguing to speculate that particular regions are poised for reactivation or increased expression of escape genes from the Xi and that loss of XIST RNA tethering at gene promoters or gene bodies facilitates gene reactivation, suggestive of a potentially novel mechanism for gene escape from XCI.

These data have intriguing implications for understanding the mechanisms for Xist RNA retention at the Xi in lymphocytes. We found that T cell subsets exhibit differences with Xist RNA localization patterns, and our RNA FISH and RNA-seq analyses using SLE patient samples suggest a correlation between robust Xist RNA signals localized at the Xi and increased fidelity of transcriptional repression. The Xist RNA-protein interactome was determined recently using proteomic and genetic screens, which revealed more than 200 proteins with known roles in transcriptional repression, RNA processing, RNA modifications, chromatin complexes, and nuclear architecture (31–34, 42). Curiously, we found that the expression of XIST interactome genes was altered in SLE patient T cells, with reduced expression of various nuclear matrix proteins important for XCI initiation. It is possible that the nuclear organization of the Xi may be disrupted in SLE lymphocytes, perhaps leading to selective gene reactivation. Future experiments will determine whether individuals with altered XIST interactomes are predisposed for SLE and whether perturbed Xi localization initiates gene expression changes that influence XIST interactome proteins to exacerbate disease.

## Methods

*Mice*. Female mice (aged 2–6 months) of various backgrounds (C57BL/6, BALB/c) were purchased from the Jackson Laboratory and were used to isolate bulk T cells (CD4$^+$, CD8$^+$), Th1 cells, and BM-derived macrophages (BMDM). Mice expressing Foxp3 and red fluorescent protein were purchased from The Jackson Laboratory (C57Bl/6-Foxp3 tm1Flc/J; strain no. 008374) were used to isolate Tregs. NZB/BINJ (strain no. 000684) and NZW/LacJ (strain no. 001058) animals were purchased from The Jackson Laboratory and mated in the School of Veterinary Medicine (University of Pennsylvania) animal facility to generate F1 mice, which spontaneous develop autoimmune phenotypes. Disease severity of NZB/W F1 mice was determined by monitoring proteinuria levels using Albustrix Reagent Strips (Siemens Diagnostics), where predisease animals were defined as negative, trace, or +; early-stage–disease animals were defined as + or ++; and late-stage–disease animals were defined as +++, ++++. All mice were maintained at the Penn Vet animal facility. Euthanasia via carbon dioxide was used for animal sacrifice prior to spleen isolation.

*Splenic T cell isolation and stimulation*. Organs were harvested on ice, and splenic naive CD3$^+$ T cells were isolated using CD3$^+$ T cell enrichment columns (R&D Systems). Mature naive CD4$^+$/CD8$^+$ T cells were cultured in RPMI-1640 (Invitrogen) containing 10% FBS (Gemini), 0.1% β-mercaptoethanol (Invitrogen), 1% nonessential amino acids (Invitrogen), 1% sodium pyruvate (Invitrogen), 1% penicillin-streptomycin (pen/strep) (Invitrogen), and 100 U/ml IL-2 (Thermo Pierce, PIRP75590). Bulk T cells were stimulated with 1 μg/ml plate-bound anti-CD3 (Bio X cell, BE0001-1-5mg) and 10 μg/ml soluble anti-CD28 (Bio X cell, clone 37.51) and then cultured for 3 days. Cells were harvested for slide preparation at days 0, 1, 2, and 3 after stimulation.

*Splenic CD8$^+$ T cell isolation*. Splenic naive CD3$^+$ T cells were isolated using CD3$^+$ T cell enrichment columns (R&D Systems), and enrichment for CD8$^+$ T cells was performed using a mouse CD8a$^+$ T cell isolation kit (Miltenyi Biotec). Naive CD8$^+$ T cells were cultured in RPMI-1640 containing 10% FBS, 0.1% β-mercaptoethanol, 1% nonessential amino acids, 1% sodium pyruvate, and 1% pen/strep. Cells were stimulated with 1 μg/ml plate-bound anti-CD3 and 10 μg/ml soluble anti-CD28 for 4 days and were harvested for slide preparation at days 0, 1, 2, 3, and 4 after activation.

*Splenic Th1 isolation and differentiation*. Splenic naive CD3$^+$ T cells were isolated using CD3$^+$ T cell enrichment columns (R&D Systems), and enrichment for CD4$^+$ T cells was performed using a mouse CD4$^+$ T Cell Isolation Kit (Miltenyi Biotec). For in vitro conversion into Th1 cells, CD4$^+$ naive T cells were cultured in RPMI-1640 containing 10% FBS, 0.1% β-mercaptoethanol, 1% nonessential amino acids, 1% sodium pyruvate, 1% pen/strep, and 100 U/ml IL-2 and stimulated with 1 μg/ml plate-bound anti-CD3, 10 μg/ml soluble anti-CD28, 10 ng/ml IL-12 (Thermo Fisher Scientific, PHC1124), and 1 μg/ml anti–IL-4 for 3 days. Cells were harvested for slide preparation at days 0, 1, 2, and 3 after stimulation.

*Splenic Treg isolation*. Treg cells were isolated 2 ways (yielding similar results): (a) by in vitro differentiation using anti-IL-4 (Bio X Cell, 11B11), anti-IFN-γ, and TGF-β1 (Thermo Fisher Scientific, PHG9214) or (b) by purifying RFP-tagged Foxp3–expressing cells. For in vitro generation of Tregs, splenic CD3$^+$ T cells were isolated using CD3$^+$ T cell enrichment columns, as described above (R&D Systems), followed by CD4$^+$ T cell enrichment using CD4$^+$ isolation columns (Miltenyi Biotec). Cells were cultured in RPMI-1640 containing 10% FBS, 0.1% β-mercaptoethanol, 1% nonessential amino acids, 1% sodium pyruvate, 1% pen/strep, and 100 U/ml IL-2 and were activated for differentiation with 1 μg/ml plate-bound anti-CD3, 10 μg/ml soluble anti-CD28, 1 μg/ml anti–IL-4, 1 μg/ml anti–IFN-γ, and 5 ng/ml TGF-β1 for 3 days. Cells were harvested for slide preparation at days 0, 1, 2, and 3 after stimulation. For isolation of mature Tregs using RFP-Foxp3 mice, splenic CD3$^+$ T cells were isolated (CD3$^+$ T cell enrichment columns; R&D Systems), followed by enrichment for CD4$^+$ T cells (Miltenyi Biotec). Foxp3$^+$ Tregs were sorted and cultured in RPMI-1640 containing 10% FBS, 0.1% β-mercaptoethanol, 1% nonessential amino acids, 1% sodium pyruvate, 1% pen/strep, and 100 U/ml IL-2, and cells were stimulated with 1 μg/ml plate-bound anti-CD3 and 10 μg/ml soluble anti-CD28 before being cultured for 3 days.

*Flow cytometry and cell sorting*. Organs were harvested on ice in FACS buffer (PBS/3% FCS), and single cell suspensions were prepared by meshing through 40-μm cell strainers; then, cells were stained with antibodies for FACS analyses. Briefly, cells were stained with fluorochrome-conjugated or biotinylated antibodies to mouse. Staining was performed in PBS/1%BSA containing mouse IgG Fc fragments (Jackson Immunoresearch, catalog 115-006-020). Dead cells and doublets were excluded and sorting was performed on a FACS Aria II machine using the following markers: Naive CD4 T cells: CD4$^+$, CD62L$^+$, CD44$^-$; active CD4 T cells: CD4$^+$, CD62L$^-$, CD44$^+$; naive CD8 T cells: CD8$^+$, CD62L$^+$, CD44$^-$; active CD8 T cells: CD8$^+$, CD62L$^-$, CD44$^+$; DN: CD4$^-$, CD8$^-$; DP: CD4$^+$, CD8$^+$; CD4 single positive (SP): CD4$^+$, CD8$^-$; CD8 SP: CD4$^-$, CD8$^+$; DN1: CD4$^-$, CD8$^-$, CD25$^-$, CD44$^+$; DN2: CD4$^-$, CD8$^-$, CD44$^+$, CD25$^+$; DN3: CD4$^-$, CD8$^-$, CD44$^-$, CD25$^+$; and DN4: CD4$^-$, CD8$^-$, CD44$^-$, CD25$^-$. Antibodies used included CD4 (H12.19, BioLegend), CD8 (53-6.7, eBioscience), CD25 (PC61, BioLegend), CD44 (IM7, BioLegend), and CD62L (MEL-14, BioLegend). Intracellular detection of FOXP3 was performed by using a FOXP3 staining buffer set (00-5523-00, eBioscience), following the protocol provided by the manufacturer.

*Xist RNA FISH and IF for H3K27me3*. Sequential RNA FISH and IF for splenocytes was performed following established protocols (21), where Xist RNA was performed first, followed by IF. For Xist RNA FISH, 2 Cy3-labeled 20-nucleotide oligo probes were designed to recognize regions within exon 1 (synthesized by IDT). For IF, cells were blocked with 0.2% PBS-Tween, 0.5% BSA. Histone H3K27me3 (Active Motif; catalog 39155) was diluted 1:100. Images were obtained using a Nikon Eclipse microscope and were categorized by the 4 types of Xist RNA localization patterns, as described previously (21, 23). Statistical significance was calculated using $\chi^2$ tests and one-way ANOVA.

*Analysis of RNA-seq data sets in SLE patients and healthy controls*. We downloaded fastq files for RNA-seq data from NCBI (NCBI Bioproject Accession ID PRJNA293549) (28). This study profiled peripheral unstimulated T cells from 2 male SLE samples, 12 female samples with SLEDAI scores ranging from 0–26, and 4 healthy female controls. RNA-seq analyses were performed using the online CyVerse platform (43, 44). Reads from each sample were aligned to human reference genome (GRCh38) using HISAT2 sequence aligner 2.1 (45) with default settings (for intron length between 20 nt and 15 kb), and

transcripts were reconstructed using Stringtie 1.3.3 with default settings (46). Transcript counts were generated by Stringtie and used for DEseq2 analysis. Data normalization and identification of differentially expressed transcripts was performed using DEseq2, which uses the median-of-ratio method of normalization to correct for sequencing depth and RNA composition (47). Filtering was carried out manually to remove unexpressed and lowly expressed transcript reads from both healthy controls and SLE samples (reads per kilobase of transcript, per million mapped reads [RPKM] < 0.5 across every sample). Differentially expressed gene transcripts (FDR < 0.05) were identified using DEseq2. Heatmaps of differentially expressed X-linked transcripts were created using normalized expression value (G-scores) and visualized using the MultiExperiment Viewer (MeV) tool (48). To identify the regions of the X-chromosome containing genes overexpressed in SLE T cells, we performed positional gene enrichment (PGE) analysis using an online PGE analysis tool (http://silico.biotoul.fr/pge/) (49). We used our list of X-linked transcripts overexpressed in all SLE patient T cells (Supplemental Table 1) (FDR < 0.05) and determined the percent enrichment for chromosome regions that were considered significantly overrepresented at significance threshold of FDR < 0.05. To identify whether regions of significant percent enrichment overlapped with known XCI escape genes, we mapped the escape regions along the human X-chromosome previously identified in ref. 50. The X-chromosome/autosome ratio was determined by calculating the RPKM for each chromosome and then dividing the X-chromosome RPKM by the mean RPKM for all autosomes.

*Statistics*. Statistical analyses were performed using Prism software version 7.0 (GraphPad). Experiments are reported as mean ± SD. Data were analyzed using 2-tailed Student's *t* test for comparison between 2 data sets or 1-way ANOVA for group comparisons for each type of Xist RNA localization pattern. Differences were considered significant at a *P* value less than 0.05.

*Study approval*. The acquisition of blood samples from pediatric SLE patients and healthy age-matched controls from the CHOP was approved by the IRB at CHOP. Written informed consent was received from participants prior to inclusion in this study. Mice were bred and maintained in the School of Veterinary Medicine in accordance with the regulations of the American Association for the Accreditation of Laboratory Animal Care. All protocols were approved by the Institutional Animal Care and Use Committee, and animal experiments were approved by the University of Pennsylvania IACUC.

## Author contributions

MCA designed the studies and wrote the manuscript, and CMS and MA edited the manuscript. CMS performed the Xist RNA FISH and IF analyses for the developing thymocytes and mature thymic T cells, which were FACS sorted and analyzed by VS and SB. CMS designed, performed, and analyzed the $CD3^+$ T cell time course experiments for Xist RNA and H3K27me3 localization. CMS performed Xist RNA FISH analyses for $CD8^+$ T cells and NZB/W F1 T cells at 3 disease states. DSH cultured Th1 and Tregs and performed Xist RNA FISH experiments and analyses. JW isolated T cells from PBMCs from pediatric SLE patients and heathy controls (recruited at CHOP by EMB) and performed XIST RNA FISH, and MCA performed the analyses. BP performed the bioinformatics analyses using published RNA-seq data and generated the heatmaps and lists of X-linked gene transcripts and XIST RNA interacting proteins that are differentially expressed.

## Acknowledgments

We would like to thank C. Hunter and J. DeLong for assistance with Th1 culture, as well as C. Berry and B. Freedman for assistance with Treg isolation. We are grateful for insightful discussions with T. Laufer, L. King, Z. Beethem, and J. Punt for data interpretation, statistical analyses, and editing of the manuscript. This research was supported by a University Research Foundation grant, American Chemical Society grant (to MCA); NIH R21 AI124084, NICHD 5K12 HD085848-03, and McCabe Foundation grant (to MCA); T32-GM007229, T32-HD083185, and F31GM123604 (to CMS); and NIH R01 AI079002 and NIH R01 GM111384 (to MLA).

Address correspondence to: Montserrat C. Anguera, Department of Biomedical Sciences, School of Veterinary Medicine, University of Pennsylvania, Room 390EB, 3800 Spruce Street, Philadelphia, Pennsylvania 19104, USA. Phone: 215.898.0567; Email: anguera@upenn.edu.

1. Eaton WW, Rose NR, Kalaydjian A, Pedersen MG, Mortensen PB. Epidemiology of autoimmune diseases in Denmark. *J Autoimmun*. 2007;29(1):1–9.
2. Liu K, et al. X Chromosome Dose and Sex Bias in Autoimmune Diseases: Increased 47,XXX in Systemic Lupus Erythematosus and Sjogren's Syndrome. *Arthritis Rheumatol*. 2016;68(5):1290–1300.
3. Cooney CM, et al. 46,X,del(X)(q13) Turner's syndrome women with systemic lupus erythematosus in a pedigree multiplex for SLE. *Genes Immun*. 2009;10(5):478–481.
4. Libert C, Dejager L, Pinheiro I. The X chromosome in immune functions: when a chromosome makes the difference. *Nat Rev Immunol*. 2010;10(8):594–604.
5. Ross MT, et al. The DNA sequence of the human X chromosome. *Nature*. 2005;434(7031):325–337.
6. Lu Q, Wu A, Tesmer L, Ray D, Yousif N, Richardson B. Demethylation of CD40LG on the inactive X in T cells from women with lupus. *J Immunol*. 2007;179(9):6352–6358.
7. Chauhan SK, Singh VV, Rai R, Rai M, Rai G. Distinct autoantibody profiles in systemic lupus erythematosus patients are selectively associated with TLR7 and TLR9 upregulation. *J Clin Immunol*. 2013;33(5):954–964.
8. García-Ortiz H, Velázquez-Cruz R, Espinosa-Rosales F, Jiménez-Morales S, Baca V, Orozco L. Association of TLR7 copy number variation with susceptibility to childhood-onset systemic lupus erythematosus in Mexican population. *Ann Rheum Dis*. 2010;69(10):1861–1865.
9. Hewagama A, et al. Overexpression of X-linked genes in T cells from women with lupus. *J Autoimmun*. 2013;41:60–71.
10. Subramanian S, et al. A Tlr7 translocation accelerates systemic autoimmunity in murine lupus. *Proc Natl Acad Sci USA*. 2006;103(26):9970–9975.
11. Pisitkun P, Deane JA, Difilippantonio MJ, Tarasenko T, Satterthwaite AB, Bolland S. Autoreactive B cell responses to RNA-related antigens due to TLR7 gene duplication. *Science*. 2006;312(5780):1669–1672.
12. Hwang SH, et al. B cell TLR7 expression drives anti-RNA autoantibody production and exacerbates disease in systemic lupus erythematosus-prone mice. *J Immunol*. 2012;189(12):5786–5796.
13. Payer B, Lee JT. X chromosome dosage compensation: how mammals keep the balance. *Annu Rev Genet*. 2008;42:733–772.
14. Brockdorff N, et al. Conservation of position and exclusive expression of mouse Xist from the inactive X chromosome. *Nature*. 1991;351(6324):329–331.
15. Brown CJ, et al. A gene from the region of the human X inactivation centre is expressed exclusively from the inactive X chromosome. *Nature*. 1991;349(6304):38–44.
16. Penny GD, Kay GF, Sheardown SA, Rastan S, Brockdorff N. Requirement for Xist in X chromosome inactivation. *Nature*. 1996;379(6561):131–137.
17. Plath K, et al. Role of histone H3 lysine 27 methylation in X inactivation. *Science*. 2003;300(5616):131–135.
18. Silva J, et al. Establishment of histone h3 methylation on the inactive X chromosome requires transient recruitment of Eed-Enx1 polycomb group complexes. *Dev Cell*. 2003;4(4):481–495.
19. Zhao J, Sun BK, Erwin JA, Song JJ, Lee JT. Polycomb proteins targeted by a short repeat RNA to the mouse X chromosome. *Science*. 2008;322(5902):750–756.
20. Jonkers I, Monkhorst K, Rentmeester E, Grootegoed JA, Grosveld F, Gribnau J. Xist RNA is confined to the nuclear territory of the silenced X chromosome throughout the cell cycle. *Mol Cell Biol*. 2008;28(18):5583–5594.
21. Wang J, Syrett CM, Kramer MC, Basu A, Atchison ML, Anguera MC. Unusual maintenance of X chromosome inactivation predisposes female lymphocytes for increased expression from the inactive X. *Proc Natl Acad Sci USA*. 2016;113(14):E2029–E2038.
22. Savarese F, Flahndorfer K, Jaenisch R, Busslinger M, Wutz A. Hematopoietic precursor cells transiently reestablish permissiveness for X inactivation. *Mol Cell Biol*. 2006;26(19):7167–7177.
23. Syrett CM, et al. Loss of Xist RNA from the inactive X during B cell development is restored in a dynamic YY1-dependent two-step process in activated B cells. *PLoS Genet*. 2017;13(10):e1007050.
24. Wells AD, Gudmundsdottir H, Turka LA. Following the fate of individual T cells throughout activation and clonal expansion. Signals from T cell receptor and CD28 differentially regulate the induction and duration of a proliferative response. *J Clin Invest*. 1997;100(12):3173–3183.
25. Sekiya T, Yoshimura A. In Vitro Th Differentiation Protocol. *Methods Mol Biol*. 2016;1344:183–191.
26. Perry D, Sang A, Yin Y, Zheng YY, Morel L. Murine models of systemic lupus erythematosus. *J Biomed Biotechnol*. 2011;2011:271694.
27. Mohan C, Datta SK. Lupus: key pathogenic mechanisms and contributing factors. *Clin Immunol Immunopathol*. 1995;77(3):209–220.
28. Bradley SJ, Suarez-Fueyo A, Moss DR, Kyttaris VC, Tsokos GC. T Cell Transcriptomes Describe Patient Subtypes in Systemic Lupus Erythematosus. *PLoS ONE*. 2015;10(11):e0141171.
29. Balaton BP, Cotton AM, Brown CJ. Derivation of consensus inactivation status for X-linked genes from genome-wide studies. *Biol Sex Differ*. 2015;6:35.
30. Wang J, Ioan-Facsinay A, van der Voort EI, Huizinga TW, Toes RE. Transient expression of FOXP3 in human activated nonregulatory CD4+ T cells. *Eur J Immunol*. 2007;37(1):129–138.
31. Minajigi A, et al. Chromosomes. A comprehensive Xist interactome reveals cohesin repulsion and an RNA-directed chromosome conformation. *Science*. 2015;349(6245):aab2276.
32. Chu C, et al. Systematic discovery of Xist RNA binding proteins. *Cell*. 2015;161(2):404–416.
33. McHugh CA, et al. The Xist lncRNA interacts directly with SHARP to silence transcription through HDAC3. *Nature*. 2015;521(7551):232–236.
34. Monfort A, et al. Identification of Spen as a Crucial Factor for Xist Function through Forward Genetic Screening in Haploid Embryonic Stem Cells. *Cell Rep*. 2015;12(4):554–561.
35. Chen CK, et al. Xist recruits the X chromosome to the nuclear lamina to enable chromosome-wide silencing. *Science*. 2016;354(6311):468–472.
36. Sunwoo H, Colognori D, Froberg JE, Jeon Y, Lee JT. Repeat E anchors Xist RNA to the inactive X chromosomal compart-

ment through CDKN1A-interacting protein (CIZ1). *Proc Natl Acad Sci USA*. 2017;114(40):10654–10659.
37. Ridings-Figueroa R, et al. The nuclear matrix protein CIZ1 facilitates localization of Xist RNA to the inactive X-chromosome territory. *Genes Dev*. 2017;31(9):876–888.
38. Wang CY, Jégu T, Chu HP, Oh HJ, Lee JT. SMCHD1 Merges Chromosome Compartments and Assists Formation of Super-Structures on the Inactive X. *Cell*. 2018;174(2):406–421.e25.
39. Csankovszki G, Nagy A, Jaenisch R. Synergism of Xist RNA, DNA methylation, and histone hypoacetylation in maintaining X chromosome inactivation. *J Cell Biol*. 2001;153(4):773–784.
40. Liu G, Li Z, Wei Y, Lin Y, Yang C, Liu T. Direct detection of FoxP3 expression in thymic double-negative CD4-CD8- cells by flow cytometry. *Sci Rep*. 2014;4:5781.
41. Cifuentes-Rojas C, Hernandez AJ, Sarma K, Lee JT. Regulatory interactions between RNA and polycomb repressive complex 2. *Mol Cell*. 2014;55(2):171–185.
42. Moindrot B, et al. A Pooled shRNA Screen Identifies Rbm15, Spen, and Wtap as Factors Required for Xist RNA-Mediated Silencing. *Cell Rep*. 2015;12(4):562–572.
43. Goff SA, et al. The iPlant Collaborative: Cyberinfrastructure for Plant Biology. *Front Plant Sci*. 2011;2:34.
44. Merchant N, et al. The iPlant Collaborative: Cyberinfrastructure for Enabling Data to Discovery for the Life Sciences. *PLoS Biol*. 2016;14(1):e1002342.
45. Kim D, Langmead B, Salzberg SL. HISAT: a fast spliced aligner with low memory requirements. *Nat Methods*. 2015;12(4):357–360.
46. Pertea M, Pertea GM, Antonescu CM, Chang TC, Mendell JT, Salzberg SL. StringTie enables improved reconstruction of a transcriptome from RNA-seq reads. *Nat Biotechnol*. 2015;33(3):290–295.
47. Love MI, Huber W, Anders S. Moderated estimation of fold change and dispersion for RNA-seq data with DESeq2. *Genome Biol*. 2014;15(12):550.
48. Saeed AI, et al. TM4: a free, open-source system for microarray data management and analysis. *BioTechniques*. 2003;34(2):374–378.
49. De Preter K, Barriot R, Speleman F, Vandesompele J, Moreau Y. Positional gene enrichment analysis of gene sets for high-resolution identification of overrepresented chromosomal regions. *Nucleic Acids Res*. 2008;36(7):e43.
50. Carrel L, Willard HF. X-inactivation profile reveals extensive variability in X-linked gene expression in females. *Nature*. 2005;434(7031):400–404.